Cylinder wakes in flowing soap films

Peter Vorobieff[1,2] and Robert E. Ecke[1]
[1]*Center for Nonlinear Studies, Condensed Matter and Thermal Physics Group, Los Alamos National Laboratory, Los Alamos, New Mexico 87545*
[2]*Dynamic Experimentation Group, Los Alamos National Laboratory, Los Alamos, New Mexico 87545*
(Received 16 February 1999)

We present an experimental characterization of cylinder wakes in flowing soap films. From instantaneous velocity and thickness fields, we find the vortex-shedding frequency, mean-flow velocity, and mean-film thickness. Using the empirical relationship between the Reynolds and Strouhal numbers obtained for cylinder wakes in three dimensions, we estimate the effective soap-film viscosity and its dependence on film thickness. We also compare the decay of vorticity with that in a simple Rankine vortex model with a dissipative term to account for air drag. [S1063-651X(99)05509-9]

PACS number(s): 47.27.Vf, 47.32.Cc, 67.70.+n, 83.85.−c

The formation and structure of the wake behind a cylinder is one of the most basic of hydrodynamic problems. In a cylinder wake, the flow pattern depends only on the Reynolds number $\mathrm{Re}=u_\infty d/\nu$ determined by the freestream velocity u_∞, the cylinder diameter d, and the fluid viscosity ν. The eddies are shed alternately from the two sides of the cylinder, forming two rows of staggered vortices (a vortex street) downstream. The vortex-street stability in an inviscid fluid was originally considered theoretically by von Karman [1]. Experiments in three dimensions (3D) show a wide range of wakes ($10^2<\mathrm{Re}<10^5$) to exhibit this vortex-street behavior. At low Re the wake is well approximated as two-dimensional [2]. Recent quantitative studies of flowing soap films [3–5] have opened up possibilities of studying such classic problems under conditions which are regarded as very two-dimensional. Thus revisiting the vortex-shedding problem in soap films provides a fundamental benchmark for the degree to which soap-film flows can be approximated as two-dimensional. Earlier attempts [6–8] to quantify such flows were limited by the range of accessible Re. An examination of the characteristics of vortex shedding over a wide range of Re would allow comparison between two-dimensional (2D) soap film flows and the three-dimensional case where spanwise perturbations can be appreciable.

In addition to its role as a fundamental problem in hydrodynamics, cylinder wake flows can help elucidate the behavior of isolated or weakly interacting vortices on a specific spatial scale. This can provide information for a better understanding of two-dimensional turbulence reported in soap films [3,4]. Experimental studies of turbulence in soap films and in other laboratory quasi-2D flows such as electron plasmas [9] and strongly stratified flows [10] have been important in understanding the nature of turbulence in two dimension and building the foundations for comparisons with other quasi-2D flows (e.g., geophysical). In soap-film studies, the value of film viscosity ν is an important source of uncertainty, because it has been only roughly estimated for a narrow range of thicknesses [11,12]. Air-drag effects lead to additional difficulty in finding the internal viscosity.

We conducted a systematic study of the dimensionless vortex-shedding frequency generated by cylinder wakes (Fig. 1) in flowing soap films as a function of cylinder diameter d, mean film thickness h, and freestream velocity u_∞. By comparing with results for 3D cylinder wake flows [13], we obtain an independent determination of film viscosity, which is consistent with the h^{-1} dependence suggested by theory [14]. Using particle-image velocimetry measurements of velocity and vorticity fields, we also determined the decay of peak vorticity. A model of the decay of a simple Rankine vortex by internal viscous dissipation gives good agreement with the experiment for smaller rod diameters ($d<1$ mm) but shows substantial deviations at larger rod diameters. This suggests that external damping associated with air drag may be important for larger scales but that internal viscous dissipation dominates at smaller length scales. Moreover, addition of an air-drag term to the vorticity decay equation results in significantly improved correspondence with the experiment for larger scales.

The dimensionless vortex-shedding frequency (the Strouhal number) is $\mathrm{St}=fd/u_\infty$, where f is the vortex-shedding frequency, or equivalently $\mathrm{St}=\lambda/d$ where λ is the vortex spacing in the mean-flow direction. An extensive study of cylinder wakes in terms of Re and St [13] produced two empirical relationships between the numbers applicable for $\mathrm{Re}<200$ and $\mathrm{Re}>200$. An intriguing possibility for using this data to infer the effective film viscosity was suggested earlier [8]. By shifting the data to match the 3D measurements one obtains surface viscosity although the earlier work did not quote a value for that viscosity.

Soap-film viscosity has contributions both from the surface layers and from the bulk of the film. A soap film is a

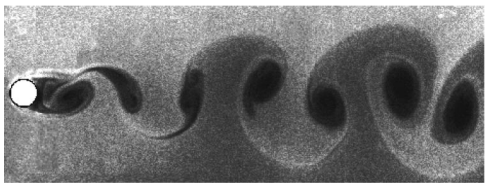

FIG. 1. Wake behind a circular cylinder (instantaneous thickness field). Peak thickness variation 35% of mean thickness. Darker areas correspond to thinner film. $d=635$ μm, $u_\infty=105$ cm/s, $h=12.7$ μm, and $\mathrm{Re}=182$ (estimation procedure for Re described in text). The field width is 14 mm.

thin (~ 10 μm) slab of water sandwiched between two monolayers of soap molecules, the hydrophobic heads of the latter protruding into the surrounding air. The resulting viscosity of the film η_f can be represented as $\eta_f = \eta_b + 2\eta_s^s/h$ (Trapeznikov [14]), where η_b is the bulk viscosity of water, η_s^s is the surface viscosity of the surface layers, and h is the thickness of the film. The thinner the film, the greater the contribution of the surface layers.

We have modified the particle-image velocimetry (PIV) technique to acquire velocity and thickness fields in flowing soap-film flows [4]. With such capabilities, we can locate the positions of vortices in the wake of the cylinder as a function of freestream velocity and film thickness through the correlation of vorticity and thickness or by direct measurement of fluid vorticity. The experimental arrangement [4,5] is similar to vertical soap-film tunnels [3], with the important difference that ours can be tilted at an arbitrary angle, providing a wider range of freestream velocities and film thicknesses. In the results presented here, the freestream velocity u_∞ was varied from 90 to 200 cm/s and the mean-film thickness values were between 4 to 20 μm. A 2% solution of household liquid soap was used.

Our visualization system employs two 500 mJ/pulse flash lamps (pulse duration, 3 μs) positioned behind the soap film, illuminating it at an angle of 45°. A 2029 by 2043 charge-coupled device (CCD) camera records images of the film in a square area 1.7 cm on a side with a spatial resolution of 8.4 μm per pixel. We use titanium dioxide particles of average size 0.2 ± 0.1 μm as the flow tracer. The volume fraction of the particles is 2×10^{-5}. Each CCD image contains two flash-illuminated exposures of the flow, separated by a variable delay τ (from 50 to 400 μs, depending on u_∞). From these images, velocity fields are extracted with a commercial PIV package [15]. 63 by 63 or 126 by 126 velocity grids were produced, with PIV interrogation window sizes being 64×64 and 32×32 correspondingly. The maximum error of the interrogation was 2.3 cm/s (2% of lowest freestream velocity). This error was primarily due to the small size of the particles barring the possibility of interrogating the flow with subpixel resolution. On the other hand, the small particle size allows us to measure film thickness simultaneously with the velocity field [4,5]. The absolute error in light intensity-derived thickness measurements is about 10% [5].

For each flow regime investigated, the data acquisition procedure was as follows: First, we measured the top reservoir discharge rate for a given thickness, acquired a velocity and thickness profile across the tunnel to verify that the lateral boundary layers near the wires were sufficiently narrow and that the flow in the central portion of the tunnel was laminar with thickness variations less than 10%. Then a cylinder was inserted into the flow and instantaneous velocity and thickness fields downstream of the cylinder were acquired. Fifteen cylinder diameters ranging from 0.1 to 2.6 mm were employed. From the velocity fields, we produced vorticity maps by numerical differentiation. As in our previous studies [4,5], we observed the vorticity concentrations to be coupled with thinner areas in the thickness field. Thus, each vortex in the vortex street manifests itself both as a concentration of vorticity and as a zone of thinned-out film in the thickness map. From either the vorticity or the thickness maps, we could measure the distance λ between peaks of same-sign vorticity or the minima of thickness corresponding to vortices being shed from the same side of the cylinder. Both the thickness and the vorticity data yield very consistent results (within the accuracy limit imposed by the grid size). λ was ensemble averaged over ten samples, and then the Strouhal number was estimated as $\mathrm{St} = \lambda/d$. Thus, for each specific pair u_∞-h, we acquired a plot of St versus d. Then we found the estimate of effective film viscosity $\nu(h)$ for each value of mean thickness h. We used $\mathrm{Re} = u_\infty d/\nu(h)$ with $\nu(h)$ as a parameter to fit our St-d results to the empirical relationship $\mathrm{St} = 0.212(1 - 21.2/\mathrm{Re})$ [8,13]. Only values of St below 0.18 were employed for fitting. Figure 2 shows the results of fitting five experimental data sets with values of h ranging from 4.7 to 18.6 μm.

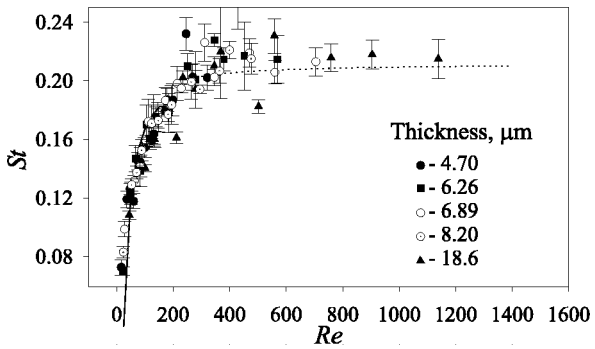

FIG. 2. Strouhal number St versus Reynolds number Re for different values of mean thickness h. Symbols corresponding to specific h values are labeled in the plot. Solid and dotted lines show 3D experimental fits: $\mathrm{St} = 0.212(1 - 21.2/\mathrm{Re})$, $\mathrm{Re} < 200$ and $\mathrm{St} = 0.212(1 - 12.7/\mathrm{Re})$, $\mathrm{Re} > 200$.

The fitting produces a ν versus h plot (Fig. 3). Also shown in the figure are the best fits approximating $\nu = \nu(h)$ with functions following Trapeznikov's formula. The two-parameter fit has the form $\nu = a/h + b$, whereas the one-parameter fit is $\nu = a/h + \nu_b$, ν_b being the bulk viscosity of water. For the range of mean thicknesses we investigated, the estimated viscosity is several times that of water and decreases with increasing thickness. The asymptotic value of ν produced by the $\nu = a/h + b$ fit as $h \to \infty$ is 1.54×10^{-2} cm^2/s, or about 1.5 the viscosity of pure water. The rms error

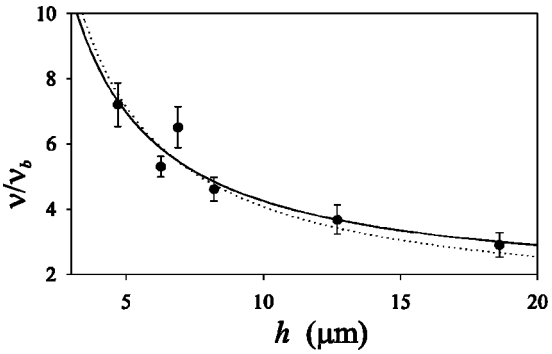

FIG. 3. Estimates of film viscosity ν nondimensionalized by bulk viscosity of water ν_b for different values of mean-film thickness h. The solid line shows the two-parameter $\nu = a/h + b$ fit through the data. The dashed line represents the one-parameter fit $\nu = a/h + \nu_b$.

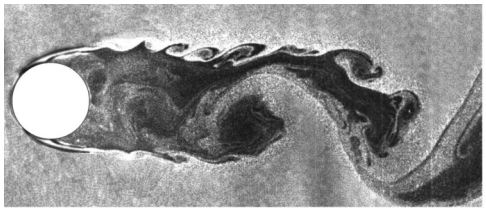

FIG. 4. Instantaneous thickness field in the wake behind a cylinder. Maximum thickness variation 50% of mean thickness, with darker areas corresponding to thinner film. $d=2590$ μm, $u_\infty=170$ cm/s, $h=12.7$ μm, $\nu=3.7\times10^{-2}$ cm^2/s, and Re$=1200$. The width of the field is 16 mm.

of the two-parameter fit is 0.54, whereas for the one-parameter fit it is 0.56. It is also of considerable interest that the value produced by these fits for $h=0.5$ μm are 0.55 (two parameters) and 0.62 cm^2/s (one parameter), consistent with the data from Couette flow-viscosity measurements [12]. Our results for thicker films (e.g. $\nu=3.7\times10^{-2}$ cm^2/s for $h=12.7$ μm) also agree with the measurements of Couder and Basdevant [11] ($\nu\simeq3\times10^{-2}$ cm^2/s for $h\sim10$ μm). Their estimate of η_s^s is 10^{-5} g/s. Our value is 1.5×10^{-5} g/s. Given the differences in specific soap solutions (soap brand and concentration), the agreement is excellent.

With the viscosity estimates produced by curve-fitting measurements for St<0.18, we can compute the value of Re for a particular freestream velocity, cylinder diameter, and mean-film thickness. For Re<200, we observe behavior analogous to that seen in 2D numerical simulations [16], and in 2D [6] and 3D [17] experiments. Instantaneous thickness maps, Fig. 1, resemble streakline-visualization images.

One basic geometric property of the wake is the ratio between the crossflow distance r between the rows of vortices shed on the alternate sides of the cylinder and the distance λ between the vortices in the freestream direction. For Re~100, ensemble-averaged data from five experimental runs yielded $r/\lambda=0.27\pm0.04$, quite close to the inviscid von Karman result of 0.281 [1]. In the far wake, the staggered vortex street breaks into an almost-parallel shear flow, from which a secondary vortex street forms. Very similar behavior for Re~150 was observed in 3D experiments [17].

As Re exceeds 200, the wakes become less stable, similar to the findings of Couder and Basdevant [11]. While one cannot claim that the wake becomes turbulent in the 3D sense (no vortex stretching, i.e., elongation of vortex tubes in the direction normal to the plane of vortex rotation in 2D), we see formation of small-scale structures in the wake, as Fig. 4 illustrates.

Returning to Fig. 2, let us consider the transition in terms of Reynolds and Strouhal numbers. The St-Re relationship for low Re follows the Re$=0.212(1-21.2/\mathrm{Re})$ line as the result of the procedure of ν estimation. As Re passes 200, there are both more scatter in the data and larger error bars. The growth of St with Re slows down considerably, and the results for Re>200 are roughly consistent with the high-Re formula Re$=0.212(1-12.7/\mathrm{Re})$, although we also get values of St higher than this 3D empirical relationship predicts. Thus, we can conclude that, similar to the 3D case, 2D cylinder wakes also undergo a transition at Re~200. The exact character of this transition and its relationship with the 3D wake transition remain the subject of future study.

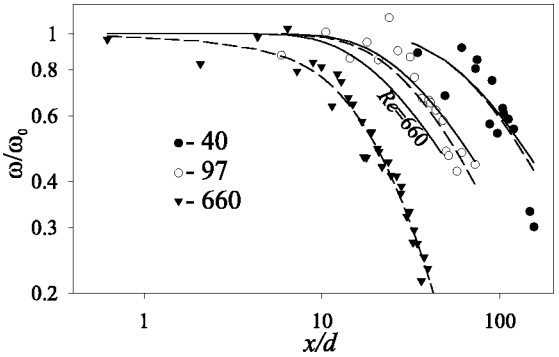

FIG. 5. Decay of normalized peak vorticity ω/ω_0 with nondimensionalized downstream distance x/d. Reynolds numbers corresponding to each group of symbols are labeled in the figure. Solid lines show best fits using the formula for Rankine vortex viscous decay, dashed lines show best fits assuming viscous decay with air drag [Eq. (3)].

A factor that must always be taken into consideration during the analysis of the soap-film data is the influence of air drag. If the film is dominated by air-drag-induced dissipation rather than internal viscous dissipation, two-dimensional Navier-Stokes equations cannot describe the flow in the film [18]. To assess the respective influence of dissipation due to air drag and to internal viscous forces, we measured the decay of vorticity with downstream distance. Figure 5 shows plots of vorticity decay for three different cylinder sizes for a fixed freestream velocity (100 cm/s) and mean-film thickness (7 μm). The data points are measurements of peak vorticity ω_m at the core of the vortices, normalized by the maximum vorticity value ω_0 immmediately downstream of the cylinder.

Assuming that the decay of vorticity arises from a combination of 2D viscous dissipation and air-drag damping with a force proportional to film velocity, one can write the vorticity decay equation as

$$\partial_t\omega+\beta\omega=\nu\nabla^2\omega. \tag{1}$$

If we further assume that the vortices are axisymmetric about their centers and that their interactions are weak, we

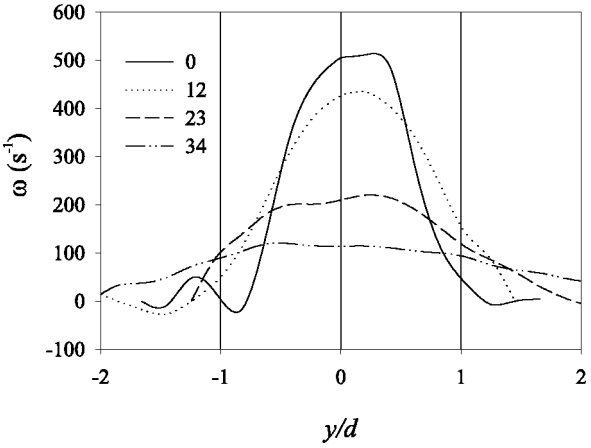

FIG. 6. Instantaneous vorticity profiles through vortex cores at different downstream locations (Re~660). Dimensionless downstream distances x/d are labeled in the graph.

can write Eq. (1) in cylindrical coordinates. Taking the intial conditions to be a simple Rankine vortex (uniform vorticity for $r<a$ and zero for $r>a$), one obtains the solution in terms of Bessel functions:

$$\frac{\omega(r,t)}{\omega_0}=\exp(-\beta t)\sum_n \frac{J_0(\alpha_n r)\exp(-\alpha_n^2 t)}{\alpha_n J_1(\alpha_n a)}, \qquad (2)$$

where α_n is the nth zero of $J_0(r)$. Considering just the peak vorticity at $r=0$, one can sum the series [19] and find the decay of peak vorticity of a Rankine vortex with both air-drag and viscous dissipation:

$$\omega(0,t)/\omega_0=\exp(-\beta t)[1-\exp(-\tau/t)], \qquad (3)$$

where $\tau=a^2/4\nu$. To compare with our data, the distance downstream x is converted to time by dividing by the channel mean velocity u_∞.

The solid lines in the plot correspond to the best fits using the expression for viscous decay of a Rankine vortex without air drag. The dashed lines depict the best fits to Eq. (3). The initial vortex radius a was constrained to remain within the range of values observed in the experiment. The restriction on the air-drag coefficient β was that the same value of β should be applicable to all data sets.

For cylinder diameters d exceeding 1 mm, the late-time decay of peak vorticity is faster than what the unmodified Rankine vortex model would suggest, whereas the model using Eq. (3) with $\beta=8\ \mathrm{s}^{-1}$ produces adequate fits for all d. Were air drag completely dominant, one would expect individual vortices to decay without spreading out in space, while viscous dissipation would cause broadening of the vortex. Figure 6 shows vorticity profiles taken through vortex cores at several downstream distances at Re$\sim$660 ($d=2.6$ mm). As the amplitude of vorticity at the core decreases, the base of the vorticity concentration widens. Thus, it seems that even for the larger-scale vortices air drag does not completely dominate internal viscous dissipation. Further investigation of the possible role of vortex interaction at higher Re and additional study of air-drag influence are certainly called for.

[1] Th. von Kármán, Göttingen Nach. Math.-Phys. Klasse 509 (1911); 547 (1912).
[2] T. Leweke and C.H.K. Williamson, Eur. J. Mech. B/Fluids **17**, 571 (1998).
[3] H. Kellay, X.-L. Wu, and W. Goldburg, Phys. Rev. Lett. **74**, 3975 (1995); **80**, 277 (1998).
[4] M. Rivera, P. Vorobieff, and R.E. Ecke, Phys. Rev. Lett. **81**, 1417 (1998).
[5] P. Vorobieff, M. Rivera, and R.E. Ecke, Phys. Fluids **11**, 2167 (1999).
[6] Y. Couder, J. Phys. (France) Lett. **45**, 353 (1984).
[7] Y. Couder, J.M. Chomaz, and M. Rabaud, Physica B **37D**, 384 (1989).
[8] M. Gharib and P. Derango, Physica D **37**, 406 (1989).
[9] T.B. Mitchell and C.F. Driscoll, Phys. Fluids **8**, 1828 (1996).
[10] J. Paret and P. Tabeling, Phys. Rev. Lett. **79**, 4162 (1997).
[11] Y. Couder and C. Basdevant, J. Fluid Mech. **173**, 225 (1986).
[12] B. Martin and X.-L. Wu, Rev. Sci. Instrum. **66**, 5603 (1995).
[13] A. Roshko, National Advisory Committee on Aeronautics (NACA) Technical Note No. 2913, 1953 (unpublished).
[14] A.A. Trapeznikov, in *Proceedings of the Second International Congress on Surface Activity*, 1957 (Butterworths, London, 1957), p. 242.
[15] VISIFLOW Analysis System, Copyright © AEA Technology, 1987–1996.
[16] P. Anagnostopoulos, J. Fluids Struc. **11**, 33 (1997).
[17] T. Karasudani and M. Funakoshi, Fluid Dyn. Res. **14**, 331 (1994).
[18] J.M. Burgess, C. Bizon, W.D. McCormick, J.B. Swift, and H.L. Swinney (unpublished).
[19] K. Terazawa, *Report of the Aeronautical Research Institute* (Tôkyô Imp. Univ., Tokyo, 1922), Vol. 1, p. 4.